General Disclaimer

One or more of the Following Statements may affect this Document

- This document has been reproduced from the best copy furnished by the organizational source. It is being released in the interest of making available as much information as possible.

- This document may contain data, which exceeds the sheet parameters. It was furnished in this condition by the organizational source and is the best copy available.

- This document may contain tone-on-tone or color graphs, charts and/or pictures, which have been reproduced in black and white.

- This document is paginated as submitted by the original source.

- Portions of this document are not fully legible due to the historical nature of some of the material. However, it is the best reproduction available from the original submission.

Produced by the NASA Center for Aerospace Information (CASI)

ANNUAL REPORT NASA GRANT NSG-1297

October 15, 1982

FRACTURE AND CRACK GROWTH IN
ORTHOTROPIC LAMINATES

Part I

Analysis of a Hybrid, Unidirectional
Laminate with Damage

Principal Investigator

James G. Goree

Department of Mechanical Engineering
College of Engineering
Clemson University
Clemson, South Carolina 29631

ANNUAL REPORT NASA GRANT NSG-1297

October 15, 1982

FRACTURE AND CRACK GROWTH IN
ORTHOTROPIC LAMINATES

Part I

Analysis of a Hybrid, Unidirectional
Laminate with Damage

Principal Investigator

James G. Goree
Professor of Mechanics and
Mechanical Engineering
Clemson University
Clemson, South Carolina   29631

Graduate Assistants

Lokeswarappa R. Dharani

Walter F. Jones

Ph.D. Candidates in
Engineering Mechanics

ABSTRACT

This study considers the development of a method of analysis capable of predicting accurately the fracture behavior of uni-directional hybrid (buffer strip) composite laminates. Three particular solutions are discussed in detail: first the case of broken fibers in a uni-directional half-plane; secondly the case of adjoined half-planes of different fiber and matrix properties and finally the solution of two half-planes bounding a third distinct region of finite width. This finite width region represents a buffer strip and primary attention is given to the potential of this strip to arrest a crack that originates in one of the half-planes.

The analysis is based on a materials modeling approach using the classical shear-lag assumption to describe the stress transfer between fibers. Explicit fiber and matrix properties of the three regions are retained and changes in the laminate behavior as a function of the relative material properties, buffer strip width and initial crack length are discussed. As an example, for a notch (broken fibers) in a graphite/epoxy laminate, the results show clearly the manner in which to select the most efficient combination of buffer strip properties necessary to arrest the crack. Ultimate failure of the laminate after crack arrest can occur under increasing load, either by continued crack extension through the buffer strip, or by fiber breakage in the undamaged half-plane. That is, for certain choices of relative material properties and width, the crack can jump the buffer strip.

As a special case of the buffer strip problem a solution is obtained for a uni-directional finite width strip containing an arbitrary number of broken fibers. The stress concentration factors for the finite width strip are compared with those for an infinite region and finite width correction factors are given.

ACKNOWLEDGEMENTS

TABLE OF CONTENTS

LIST OF TABLES

LIST OF FIGURES

CHAPTER I

INTRODUCTION

In the design and use of large composite panels in structures such as aircraft and space vehicles a major concern is the ability of the panel to function (continue to carry a substantial part of its design load) after being damaged. One technique that has evolved from the stringer reinforced metallic panel is the buffer strip or hybrid panel shown in Figure 1. Because of the fabrication methods used in composites it is possible to make such a laminate by replacing specific fibers, usually parallel to the load axes, with fibers of the appropriate physical and geometric properties necessary to arrest a crack that originates in the parent laminate material. Since the buffer strips are usually narrow and relatively far apart the stiffness, weight, and strength of the undamaged laminate is not significantly effected by the replacement.

Much experimental work has been done to investigate this behavior, i.e. to determine the best buffer strip material, with the studies of Eiseman and Kaminski [1], Hess, Huang and Rubin [2], Avery and Porter [3], Verette and Labor [4], and Poe and Kennedy [5] being significant contributions in this area. The same cannot be said for published analytical solutions and it is this question that is considered in the present study.

Some of the first work in modeling a uni-directional composite containing broken fibers was presented by Hedgepeth [6] where the case of no additional damage other than the initial notch was considered. This study was extended by Hedgepeth and Van Dyke for the special case of one

main laminate

buffer strip

original
plies in
the parent
laminate

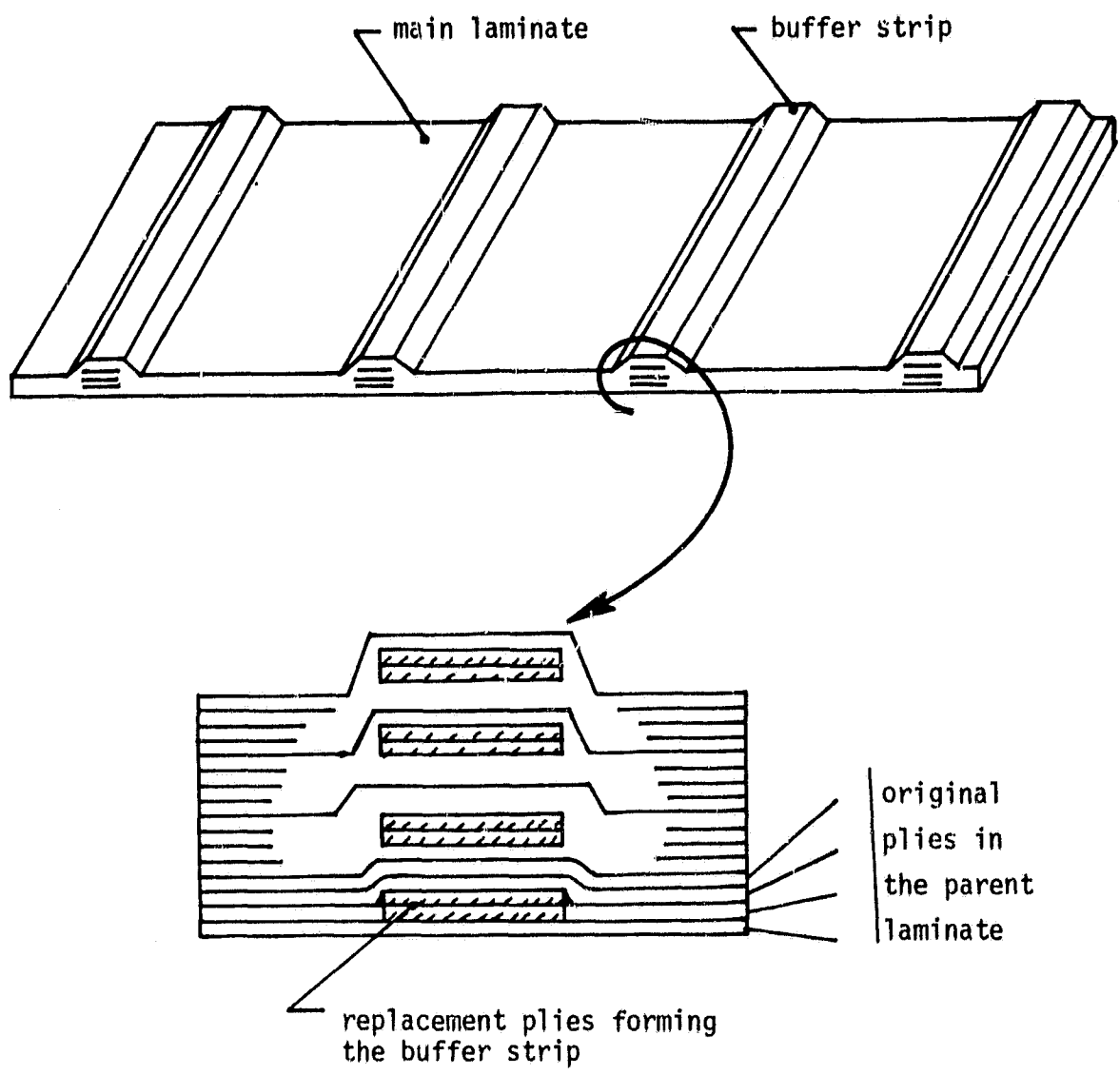replacement plies forming
the buffer strip

Figure 1. A Typical Buffer Strip Laminate Configuration

broken fiber with matrix yielding parallel to the fiber [7] and for one fiber with longitudinal splitting in the matrix [8]. Goree and Gross [9] extended the Hedgepeth solutions to include longitudinal matrix yielding and splitting for an arbitrary number of broken fibers. The results of Goree and Gross gave very good agreement with experimental results for brittle matrix composites which exhibit large longitudinal matrix splitting. For ductile matrix composites such as boron/aluminum, which exhibit large yielding but very little splitting in the matrix, this model predicted the right trend but the agreement was not very good, especially for short notch lengths. Goree, Dharani and Jones [10] attempted two modifications to the above solution. First, the matrix was assumed to be strain-hardening and secondly, a cover sheet was included over the main laminate. The results of [10] showed that the inclusion of either a strain-hardening matrix or the addition of a cover sheet did not improve the agreement between the predicted and experimental results. Based on the observed fact that in addition to longitudinal yielding of the matrix, a certain amount of stable transverse extension of the initial notch under increasing applied load takes place, Dharani, Jones and Goree [11] then extended the solution of [9] to include transverse damage ahead of the initial notch in addition to the longitudinal matrix damage. The results of [11] showed a very significant improvement in the ability of the model to represent the behavior of a ductile matrix composite.

In all these analytical studies the laminate is modeled as a two-dimensional region having a single row (mono-layer) of parallel, identical, equally spaced fibers, separated by matrix. The damage is taken to

consist of an arbitrary number of broken fibers such that all breaks lie along the x-axis, but they need not form a continuous break (notch). The fibers are assumed to be of much higher strength and extensional stiffness than the matrix and all the axial load is assumed to be carried by the fibers, with the matrix transfering load by shear stresses as given by the classical shear-lag assumption. One very important feature of the shear-lag assumption is that is simplifies the equilibrium equations by removing the transverse displacement dependence from the longitudinal equilibrium equation. The fiber stress and matrix shear stress can then be determined without solving the transverse equation.

The methods of analysis developed and discussed in the above studies [6-11] are extended in the present work to determine the stresses and displacements in a hybrid uni-directional laminate having an initial notch in the vicinity of a single finite width region of different material properties as shown in Figure 2. This geometry is an idealization of the usual periodic placement of buffer strips as indicated in Figure 1 and it is assumed that the stresses near the notch tip and the single buffer strip are approximately the same as those in a wide panel with relatively narrow buffer strips.

Of particular interest is the investigation of the behavior of the laminate as a function of the relative ultimate stress and extensional modulus of the buffer strip fibers, the buffer strip width and initial notch length.

As an initial step in understanding the basic mechanism of crack growth and arrest in a hybrid laminate, the main thrust of the investigation will be to study the behavior of the laminate as a function of the design parameters; fiber/matrix properties, buffer strip geometry and
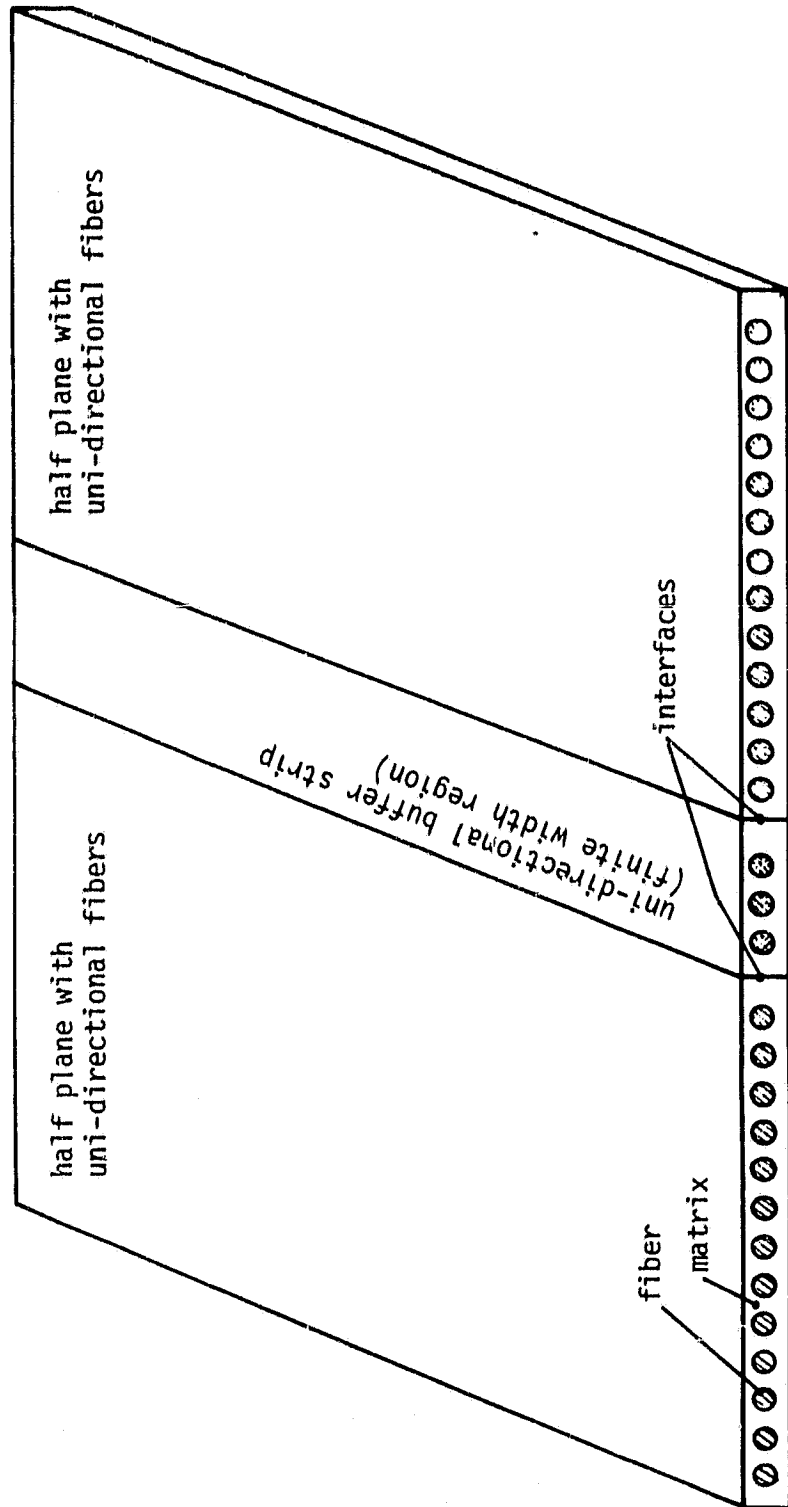
Figure 2. Idealized Buffer Strip Laminate

the initial crack length. In order to simplify the analysis, the effect of any additional damage, e.g. longitudinal matrix yielding and splitting [9] or transverse matrix and fiber damage [11] will not be considered.

A typical buffer strip laminate usually contains angle plies as well as zero degree plies. It is felt, however, that much of the characteristic behavior of the buffer strip region can be represented by the uni-directional laminate, as a major portion of the load is carried by these fibers. It appears that a primary function of the angle plies is to prevent longitudinal matrix splitting in a brittle matrix such as epoxy. This can be accounted for to some degree in the present solution by allowing the matrix to support large strains without splitting.

The presentation of the solution will follow the order of the development by the author as this seems to indicate more clearly the significant points of the analysis. Results will, however, only be given for the final solutions corresponding to the buffer strip laminate and the finite width strip. First the solution for a crack in a half-plane having arbitrary shear stresses applied to the free-edge, (which forms the basis for all the later solutions), will be developed. By matching boundary conditions along the interface, the solution for two different adjoined half-planes will be given and then the adjoined half-plane solution will be modified to account for a second interface, resulting in the buffer strip problem. The case of the finite width strip with broken fibers is obtained as a special case of the buffer strip problem by setting the shear stresses along the two interfaces to zero. These solutions are all presented in Chapter II. Chapter III deals with the numerical

technique used to solve a system of linear algebraic simultaneous equations coupled with a set of linear Fredholm integral equations of the second kind. A special method developed to evaluate accurately integrals having a cusp is emphasized. Chapter IV gives results and conclusions for the buffer strip problem and the finite width strip.

CHAPTER II

FORMULATION

Uni-Directional Half-Plane with Broken Fibers

A uni-directional array of parallel fibers with an arbitrary number of broken fibers in the form of a notch is shown in Figure 3. The laminate is subjected to a prescribed shear stress, $\tau_a(y)$, along the free edge in addition to a remote uniform tensile stress in the axial direction. Fiber breaks occur along the x-axis (axis of symmetry) and, since the loading is symmetric, only the upper half of the laminate is considered in the analysis.

The fibers are taken to be of much higher strength and extensional stiffness than the matrix and therefore all of the axial load is assumed to be carried by the fibers with the matrix transferring load by shear stresses as given by the classical shear-lag assumption. The axial fiber stress, $\sigma_n(y)$, and matrix shear stress, $\tau_n(y)$, are then given by the simple relations

$$\sigma_n(y) = E_F \frac{dv_n(y)}{dy} \quad , \quad \text{and}$$

$$\tau_n(y) = \frac{G_M}{h} [v_n(y) - v_{n-1}(y)] \ . \tag{1}$$

Where $v_n(y)$ is the axial displacement of the fiber n at the location y, E_F is the Young's modulus of the fiber, G_M is the equivalent matrix shear modulus and h is a shear transfer distance. Because of the interference between fibers it is unlikely that G_M will be the homogeneous matrix shear modulus or h the actual fiber spacing, and it is
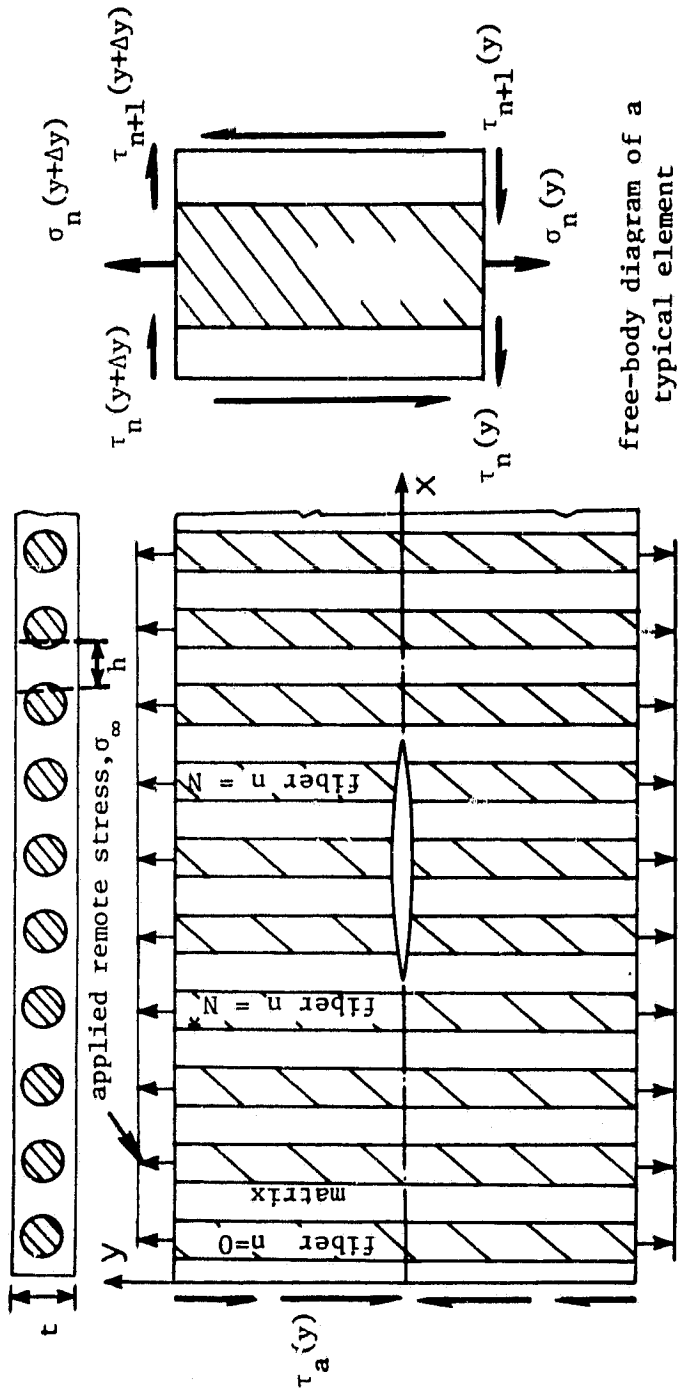
Figure 3. Uni-Directional Half-Plane with Broken Fibers

pointed out in [10] that these values should be determined experimentally for a given laminate. It is also shown in [10] that a single experiment giving the crack opening displacement as a function of applied load is sufficient to determine both the equivalent shear modulus G_M and the shear transfer distance h for a particular laminate, independent of the notch length. That is, these parameters are material constants and depend only on the fiber and matrix properties and the fiber volume fraction but not on the sizes of the damage.

By virtue of the shear-lag assumption the longitudinal and transverse equilibrium equations become decoupled and the fiber axial displacements and stresses can be obtained without solving the transverse equilibrium equation. Therefore, only the equilibrium equation in the longitudinal (axial) direction will be considered. With reference to the free-body diagram of a typical fiber-matrix region shown in Figure 3, the equilibrium equations in the longitudinal direction is given by

$$\frac{A_F}{t} \frac{d\sigma_n(y)}{dy} + \tau_{n+1}(y) - \tau_n(y) = 0 , \tag{2}$$

for all fibers except n = 0, and

$$\frac{A_F}{t} \frac{d\sigma_0(y)}{dy} + \tau_1(y) - \tau_a(y) = 0 , \quad \text{for fiber 0 .} \tag{3}$$

Using the stress-displacement relations, Equation (1), in the above equilibrium equations, the following set of differential-difference equations is obtained:

$$\frac{A_F E_F h}{G_M t} \frac{d^2 v_n}{dy^2} + v_{n+1} - 2v_n + v_{n-1} = 0 , \quad \text{and} \tag{4}$$

$$\frac{A_F E_F h}{G_M t} \frac{d^2 v_0}{dy^2} + v_1 - v_0 = \tau_a(y) . \tag{5}$$

Noting the coefficient of the second derivative term in the above equations, the following changes in the variables are suggested:

$$\text{let} \quad y = \sqrt{\frac{A_F E_F h}{G_M t}} \; \eta \; ,$$

$$\sigma_n = \sigma_\infty \bar{\sigma}_n = E_F \frac{dv_n}{dy} \; , \quad \text{and}$$

$$v_n = \sigma_\infty \sqrt{\frac{A_F h}{E_F G_M t}} \; V_n \; . \tag{6}$$

Algebraic manipulation then gives

$$\sigma_n = \sigma_\infty \frac{dV_n}{d\eta} \quad \text{and} \quad \tau_n = \sigma_\infty \sqrt{\frac{G_M A_F}{E_F h t}} \; (V_n - V_{n-1}) \; , \tag{7}$$

where, η , $\bar{\sigma}_n$ and $V_n(\eta)$ are non-dimensional.

The resulting equilibrium equations in non-dimensional form are given by

$$\frac{d^2 V_n}{d\eta^2} + V_{n+1} - 2V_n + V_{n-1} = 0 \; , \quad \text{and} \tag{8}$$

$$\frac{d^2 V_0}{d\eta^2} + V_1 - V_0 = \bar{\tau}_a(\eta) \; , \tag{9}$$

where,

$$\bar{\tau}_a(\eta) = \sqrt{\frac{E_F t h}{A_F G_M}} \; \frac{\tau_a(y)}{\sigma_\infty} \; .$$

These differential-difference equations are reduced to differential equations by introducing the even valued transform as

$$\bar{V}(\eta,\theta) = \sum_{n=0}^{\infty} V_n(\eta) \cos[(n+\tfrac{1}{2})\theta] \; , \tag{10}$$

from which

$$V_n(\eta) = \frac{2}{\pi} \int_0^\pi \bar{V}(\eta,\theta)\cos[(n+\tfrac{1}{2})\theta]d\theta \; . \tag{11}$$

Making use of the above transformation and the orthogonality property of

the circular functions, the two equilibrium equations may be written as one equation valid for all values of n and η as follows:

$$\frac{2}{\pi}\int_0^\pi \left\{ \frac{d^2\bar{V}}{d\eta^2} - 2[1-\cos(\theta)]\bar{V} \right\} \cos[(n+\tfrac{1}{2})\theta]d\theta$$

$$= \frac{2}{\pi}\int_0^\pi \bar{\tau}_a(\eta)\cos(\theta/2)\cos[(n+\tfrac{1}{2})\theta]d\theta \ ,$$

which is of the form

$$\frac{2}{\pi}\int_0^\pi F(\eta,\theta)\cos[(n+\tfrac{1}{2})\theta]d\theta = 0 \quad \text{for all } \eta \text{ and n} .$$

Noting the definition of $\bar{V}(\eta,\theta)$ in Equation (10) and (11) it is seen that the function $F(\eta,\theta)$ is even valued in θ and therefore, if the integral is to vanish for all η, the function $F(\eta,\theta)$ must be zero. The single equation specifying $\bar{V}(\eta,\theta)$ is then

$$\frac{d^2\bar{V}}{d\eta^2} - \delta^2\bar{V} = \bar{\tau}_a(\eta)\cos(\theta/2) \ , \tag{12}$$

where, $\delta^2 = 2[1-\cos(\theta)] = 4\sin^2(\theta/2)$.

The solution to the problem of vanishing stresses and displacements at infinity and uniform compression on the ends of the broken fibers will now be sought. The complete solution is obtained by adding the results corresponding to uniform axial stress and no broken fibers to the following solution. The appropriate boundary conditions are as follows:

$$V_n(\eta) = 0 \ , \quad \frac{dV_n(\eta)}{d\eta} = 0 \ , \quad \text{as } \eta \to \infty, \text{ for all fibers,} \tag{13}$$

$$\frac{dV_n(\eta)}{d\eta} = \bar{\sigma}_n(\eta) = -1 \ , \quad \text{at } \eta = 0 \ , \quad \text{for all broken fibers,} \tag{14}$$

$$V_n(\eta) = 0 \ , \quad \text{at } \eta = 0 \ , \quad \text{for all unbroken fibers.} \tag{15}$$

The complete solution to Equation (12), satisfying vanishing stresses and displacements at infinity, is given by

$$\bar{V}(\eta,\theta) = A(\theta)e^{-\delta\eta} - \frac{\cos(\theta/2)}{\delta} \int_{\eta}^{\infty} \sinh[\delta(\eta-t)]\bar{\tau}_a(t)dt \, , \tag{16}$$

where the function $A(\theta)$ is yet unknown. The remaining two boundary conditions give

$$\frac{dV_n(0)}{d\eta} = \frac{2}{\pi} \int_{0}^{\pi}[-\delta A(\theta) - \cos(\theta/2)\int_{0}^{\infty} \cosh(\delta t)\bar{\tau}_a(t)dt]\cos[(n+\tfrac{1}{2})\theta]d\theta = -1, \tag{17}$$

for all broken fibers, and

$$V_n(0) = \frac{2}{\pi} \int_{0}^{\pi} [A(\theta) + \frac{\cos(\theta/2)}{\delta} \int_{0}^{\infty} \sinh(\delta t)\bar{\tau}_a(t)dt]\cos[(n+\tfrac{1}{2})\theta]d\theta = 0 \, , \tag{18}$$

for all unbroken fibers. Equation (18) is solved exactly by taking

$$A(\theta) + \frac{\cos(\theta/2)}{\delta} \int_{0}^{\infty} \sinh(\delta t)\bar{\tau}_a(t)dt = \sum_{m=1}^{M} B_m \cos[(N^*+m+\tfrac{1}{2})\theta] \, , \tag{19}$$

where, M is the number of broken fibers. By eliminating $A(\theta)$ between equations (17) and (19), the stress boundary condition reduces to

$$\frac{2}{\pi} \int_{0}^{\pi} \sum_{m=1}^{M} B_m \cos[(N^*+m+\tfrac{1}{2})\theta]\cos[(n+\tfrac{1}{2})\theta]\delta d\theta$$

$$+ \frac{2}{\pi} \int_{0}^{\pi} \cos(\theta/2)\cos[(n+\tfrac{1}{2})\theta] \int_{0}^{\infty} e^{-\delta t}\bar{\tau}_a(t)dt \, d\theta = 1, \tag{20}$$

for $n = N^* + 1,\ldots,N$.

For a given shear stress distribution, $\bar{\tau}_a(t)$, Equation (20) reduces to a set of linear algebraic equations in the Fourier constants B_m. From Equations (16) and (19), $A(\theta)$ may be eliminated to obtain $\bar{V}(\eta,\theta)$ in terms of the constants B_m. Recalling the relation between $\bar{V}(\eta,\theta)$ and $V_n(\eta)$, an expression can be obtained for the axial fiber displacement $V_n(\eta)$ as

$$V_n(\eta) = \frac{2}{\pi} \int_{0}^{\pi} e^{-\delta\eta} \sum_{m=1}^{M} B_m \cos[(N^* + m + \tfrac{1}{2})\theta]\cos[(n+\tfrac{1}{2})\theta]d\theta$$

$$- \frac{1}{\pi} \int_{0}^{\pi} \frac{\cos(\theta/2)}{\delta} \int_{0}^{\infty} D(\delta,\eta,t) \, \bar{\tau}_a(t)dt \, \cos[(n+\tfrac{1}{2})\theta]d\theta \, , \tag{21}$$

where $D(\delta,\eta,t) = e^{-\delta|\eta-t|} - e^{-\delta(\eta+t)}$.

The axial fiber stress is obtained by differentiating Equation (21) with respect to η and is given by

$$\bar{\sigma}_\eta = \frac{dV_\eta(\eta)}{d\eta}$$

$$= -\frac{2}{\pi} \int_0^\pi \delta e^{-\delta\eta} \sum_{m=1}^M B_m \cos[(N^* + m + \tfrac{1}{2})\theta]\cos[(n + \tfrac{1}{2})\theta]d\theta$$

$$-\frac{1}{\pi} \int_0^\pi \cos(\theta/2) \int_0^\infty \left\{ e^{-\delta(\eta+t)} - p\, e^{-\delta|\eta-t|} \right\} \bar{\tau}_a(t)dt \cos[(n + \tfrac{1}{2})\theta]d\theta,$$

$$(21a)$$

where, $p = 1$ for $t \leq \eta$, and

$p = -1$ for $t > \eta$.

Adjoined Uni-Directional Half-Planes

Figure 4 shows two uni-directional half-planes of different fiber and matrix properties which are assembled to form adjoined half-planes. Both planes may have an arbitrary number of broken fibers. Superscripts I and II are used to designate quantities corresponding to plane I and II respectively. The normalized spatial variables, η and ξ, in the longitudinal direction are related by

$$\sqrt{\left(\frac{A_F E_F h}{G_M t}\right)^I}\, \eta = \sqrt{\left(\frac{A_F E_F h}{G_M t}\right)^{II}}\, \xi = y .$$

$$(22)$$

The shear stresses, $\bar{\tau}_a^I(\eta)$ and $\bar{\tau}_a^{II}(\xi)$, at the interface are normalized with respect to material properties of plane I and II respectively, and are related to the actual shear stresses as follows:

$$\bar{\tau}_a^I(\eta) = \sqrt{\left(\frac{E_F th}{A_F G_M}\right)^I}\, \frac{\tau_a^I(y)}{\sigma_\infty^I} , \quad \text{and}$$

Figure 4. Adjoined Uni-Directional Half-Planes

$$\bar{\tau}_a^{II}(\xi) = \sqrt{\left(\frac{E_F th}{A_F G_M}\right)^{II} \frac{\tau_a^{II}(y)}{\sigma_\infty^{II}}} \quad , \tag{23}$$

where, $\tau_a^I(y)$ and $\tau_a^{II}(y)$ are the actual shear stresses at the interface acting on plane I and II. Since the remote displacements and hence the remote strains are assumed equal, the remote stresses in planes I and II must be related by

$$\frac{\sigma_\infty^I}{E_F^I} = \frac{\sigma_\infty^{II}}{E_F^{II}} \quad . \tag{24}$$

If $\bar{\tau}_a^I(\eta)$ and $\bar{\tau}_a^{II}(\xi)$ are known then the solution for each of the half-planes is the same as that developed in the previous section, Equation (20). The Fourier constants B_m^I and B_m^{II} corresponding to broken fibers in plane I and II can then be obtained by solving the following sets of equations for known $\bar{\tau}_a^I(\eta)$ and $\bar{\tau}_a^{II}(\xi)$:

$$\sum_{m=1}^{M_1} B_m^I \frac{2}{\pi} \int_0^\pi \cos[(N^*_1 + m + \tfrac{1}{2})\theta]\cos[(n+\tfrac{1}{2})\theta]\delta d\theta$$

$$+ \frac{2}{\pi} \int_0^\pi \cos(\theta/2)\cos[(n+\tfrac{1}{2})\theta]\int_0^\infty e^{-\delta t} \bar{\tau}_a^I(t)dt\, d\theta = 1 \ ,$$

$$\text{and} \quad \sum_{m=1}^{M_2} B_m^{II} \frac{2}{\pi} \int_0^\pi \cos[(N^*_2 + m + \tfrac{1}{2})\theta]\cos[(\ell+\tfrac{1}{2})\theta]\delta d\theta \ ,$$

$$+ \frac{2}{\pi} \int_0^\pi \cos(\theta/2)\cos[(\ell+\tfrac{1}{2})\theta]\int_0^\infty e^{-\delta t} \bar{\tau}_a^{II}(t)dt\, d\theta = 1, \tag{25}$$

for $n = N^*_1 + 1,\ N^*_1 + 2, \ldots, N_1$ and $\ell = N^*_2 + 1,\ N^*_2 + 2, \ldots, N_2$, where, M_1 and M_2 are the number of broken fibers in planes I and II. The normalized displacements of a fiber in plane I and II are then given by

$$V_n^I(\eta) = \frac{2}{\pi} \int_0^\pi \sum_{m=1}^{M_1} B_m^I \cos[(N^*_1 + m + \tfrac{1}{2})\theta]\cos[(n+\tfrac{1}{2})\theta]e^{-\delta\eta} d\theta$$

$$- \frac{1}{\pi} \int_0^\pi \frac{\cos(\theta/2)}{\delta} \cos[(n+\tfrac{1}{2})\theta] \int_0^\infty D(\delta,\eta,t)\, \bar{\tau}_a^I(t)dt\, d\theta , \tag{26}$$

and $\quad V_n^{II}(\xi) = \frac{2}{\pi} \int_0^{\pi} \sum_{m=1}^{M_2} B_m^{II} \cos[(N_2^* + m + \frac{1}{2})\theta]\cos[(n+\frac{1}{2})\theta]e^{-\delta\xi} \, d\theta$

$$- \frac{1}{\pi} \int_0^{\pi} \frac{\cos(\theta/2)}{\delta} \cos[(n+\frac{1}{2})\theta] \int_0^{\infty} D(\delta,\xi,s) \; \bar{\tau}_a^{II}(s)ds \; d\theta, \quad (27)$$

where

$$v_n^I(y) = \sqrt{\left(\frac{A_F h}{E_F G_M t}\right)^I} \; \sigma_\infty^I V_n^I(\eta) \;, \quad \text{and}$$

$$v_n^{II}(y) = \sqrt{\left(\frac{A_F h}{E_F G_M t}\right)^{II}} \; \sigma_\infty^{II} V_n^{II}(\xi) \;. \quad (28)$$

When the above two half-planes are joined together the shear stress along the interface is unknown, but from equilibrium the shear stresses $\tau_a^I(y)$ and $\tau_a^{II}(y)$ acting on each of these two half-planes must be equal and opposite. Further, as the shear stress is directly related to the distortion of the matrix from the shear-lag assumption, it follows that these stresses must be proportional to the difference in the displacement of the first fibers of plane I and II. These conditions result in the following two equations:

$$\tau_a^I(y) = -\tau_a^{II}(y), \quad \text{and} \quad (29)$$

$$\tau_a^I(y) = (G_M/h)^i \left[v_0^I(y) - v_0^{II}(y) \right] \;, \quad (30)$$

where, $(G_M/h)^i$ is the equivalent shear stiffness of the interface. It is interesting to note that in a continuous elasticity solution one would match surface tractions and displacements at the interface while in the present discrete modeling solution the shear stresses are required to be equal and the shear-lag relation, Equation (30), takes the place of the displacement equality.

Substituting for the actual displacements in terms of normalized values using Equation (28), and recalling the relation between the actual and normalized shear stresses from Equation (23), Equations (29) and (30) reduce to

$$\bar{\tau}_a^{II}(\xi) = - (G_M/h)^I (h/G_M)^{II} \bar{\tau}_a^I(\eta)/R_1 , \quad \text{and} \tag{31}$$

$$\bar{\tau}_a^I(\eta) = \left[V_0^I(\eta) - R_1 V_0^{II}(\xi) \right] (G_M/h)^i /(G_M/h)^I \tag{32}$$

where,

$$R_1 = \sqrt{\left(\frac{A_F E_F h}{G_M t}\right)^{II} \left(\frac{G_M t}{A_F E_F h}\right)^I} \quad . \tag{33}$$

Using Equations (26) and (27), $V_n^I(\eta)$ and $V_n^{II}(\xi)$ can b $\quad$ d and substituted into Equation (32) thus resulting in an integra﹍ $\quad$ ﹍n for $\bar{\tau}_a^I(\eta)$ in terms of the Fourier constants, B_m^I and B_m^{II}, and the normalized shear stresses, $\bar{\tau}_a^I(\eta)$ and $\bar{\tau}_a^{II}(\xi)$. The spatial variable ξ and the normalized shear stress $\bar{\tau}_a^{II}(\xi)$ may be eliminated from the above integral equation and also from the equations for the Fourier constants, Equation (25), resulting in the following set of governing equations; two series equations and one linear integral equation:

$$\sum_{m=1}^{M_1} B_m^I \frac{2}{\pi} \int_0^\pi \cos[(N_1^* + m + \frac{1}{2})\theta]\cos[(n + \frac{1}{2})\theta]\delta d\theta$$

$$+ \frac{2}{\pi} \int_0^\pi \cos(\theta/2)\cos[(n + \frac{1}{2})\theta] \int_0^\infty e^{-\delta t} \bar{\tau}_a^I(t)dt \, d\theta = 1 , \tag{34}$$

$$\sum_{m=1}^{M_1} B_m^{II} \frac{2}{\pi} \int_0^\pi \cos[(N_2^* + m + \frac{1}{2})\theta]\cos[(\ell + \frac{1}{2})\theta]\delta d\theta$$

$$- \frac{G_{12}}{R_1^2} \frac{2}{\pi} \int_0^\pi \cos(\theta/2)\cos[(\ell + \frac{1}{2})\theta] \int_0^\infty e^{-\delta_1 t} \bar{\tau}_a^I(t)dt \, d\theta = 1 , \tag{35}$$

for $n = N_1^* + 1,...,N_1$ and $\ell = N_2^* + 1,...,N_2$, and

$$\bar{\tau}_a^I(\eta) = G_{11} \frac{2}{\pi} \int_0^\pi \sum_{m=1}^{M_1} B_m^I \cos[(N_1^* + m + \frac{1}{2})\theta]\cos(\theta/2)e^{-\delta\eta} d\theta$$

$$- R_1 G_{11} \frac{2}{\pi} \int_0^\pi \sum_{m=1}^{M_2} B_m^{II} \cos[(N_2^* + m + \frac{1}{2})\theta]e^{-\delta_1\eta} d\theta$$

$$- G_{11} \int_0^\infty \frac{2}{\pi} \int_0^\pi \frac{\cos^2(\theta/2)}{\delta} \left[D(\delta,\eta,t) + \frac{G_{11}}{R_1} D(\delta_1,\eta,t) \right] d\theta \, \bar{\tau}_a^I(t)dt$$

(36)

where, $G_{11} = (G_M/h)^i(h/G_M)^I$, $G_{12} = (G_M/h)^I(h/G_M)^{II}$ and $\delta_1 = \delta/R_1$.

The Buffer Strip Laminate

Figure 5 shows a finite width strip (buffer strip) between two half-planes of different or of the same fiber and matrix properties. One of the half-planes, plane I, and the finite strip, region II, may contain an arbitrary number of broken fibers. The normalized spatial variables η, ξ and ζ are related to each other in the same way as in Equation (22). The normalized shear stresses $\bar{\tau}_a^I(\eta)$, $\bar{\tau}_a^{II}(\xi)$, $\bar{\tau}_b^{II}(\xi)$ and $\bar{\tau}_b^{III}(\zeta)$ are related to their corresponding actual shear stresses in the same manner as in Equation (23). Further, the remote strains in all three regions are assumed equal.

The solutions for planes I and III can be obtained for known $\bar{\tau}_a^I(\eta)$ and $\bar{\tau}_b^{III}(\zeta)$ from the half-plane solution and therefore we need to determine the solution for the finite strip, region II, only. This solution is developed by considering the half-plane shown in Figure 3 with the following special condition. It may be assumed that the matrix between the fiber Nw and (Nw + 1) splits all the way to infinity and that an external shear stress $\tau_b^{II}(y)$ is applied on the surface of the split
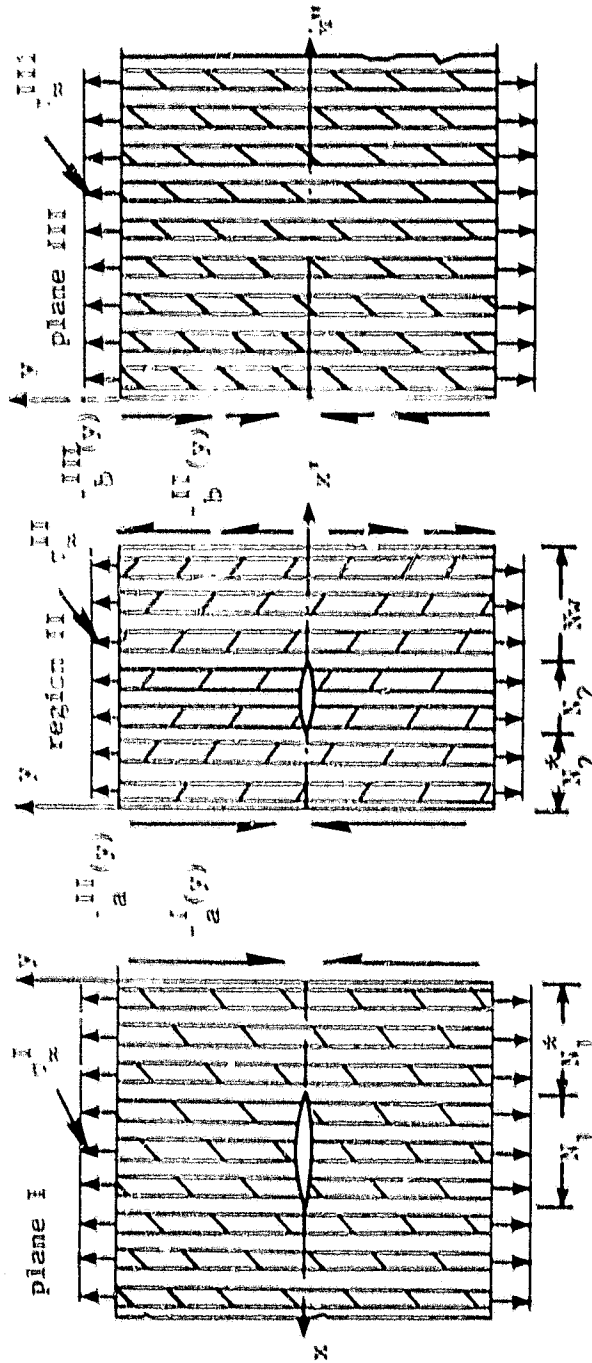
Figure 5.   The Three Regions of the Buffer Strip Laminate

as shown in Figure 6. The introduction of a split with or without the external applied shear stress results in two special equilibrium equations for the two fibers on either side of the split [9, 10, 11] in addition to those valid for the free-edge fiber and the generic fiber, n, given by Equations (8) and (9). These equilibrium equations in the normalized form are as follows:

$$\frac{d^2 V_0^{II}}{d\xi^2} + V_1^{II} - V_0^{II} = \bar{\tau}_a^{II}(\xi) \qquad , \quad \text{for fiber 0} \quad , \tag{37}$$

$$\frac{d^2 V_n^{II}}{d\xi^2} + V_{n+1}^{II} - 2V_n^{II} + V_{n-1}^{II} = 0 \quad , \quad \text{for fiber n} \quad , \tag{38}$$

$$\frac{d^2 V_{Nw}^{II}}{d\xi^2} - V_{Nw}^{II} + V_{Nw-1}^{II} = - \bar{\tau}_b^{II}(\xi) \quad , \quad \text{for fiber Nw} \quad , \quad \text{and} \tag{39}$$

$$\frac{d^2 V_{Nw+1}^{II}}{d\xi^2} + V_{Nw+2}^{II} - V_{Nw+1}^{II} = \bar{\tau}_b^{II}(\xi) \quad , \quad \text{for fiber Nw + 1} \quad . \tag{40}$$

The left hand sides of Equation (39) and (40) can be reduced to the standard form by adding or subtracting a term $(V_{Nw+1}^{II} - V_{Nw}^{II})$ on both sides. Making use of the transforms similar to Equation (10) and (11) and following the procedure of the half-plane problem, the single equation specifying the transformed normalized displacement $\bar{V}^{II}(\xi,\theta)$ can be obtained as

$$\frac{d^2 \bar{V}^{II}(\xi,\theta)}{d\xi^2} - \delta^2 \bar{V}^{II}(\xi,\theta) = \bar{\tau}_a^{II}(\xi) \cos(\theta/2) + [g(\xi) - \bar{\tau}_b^{II}(\xi)]F^2 \quad , \tag{41}$$

where,

$$g(\xi) = V_{Nw+1}^{II} - V_{Nw}^{II} \quad , \quad \text{and} \quad F^2 = \cos[(Nw + \frac{1}{2})\theta] - \cos[(Nw + \frac{3}{2})\theta] \quad .$$

The solution to Equation (41) satisfying vanishing stresses and displacements at infinity and unit compression on the crack surface is then given by:
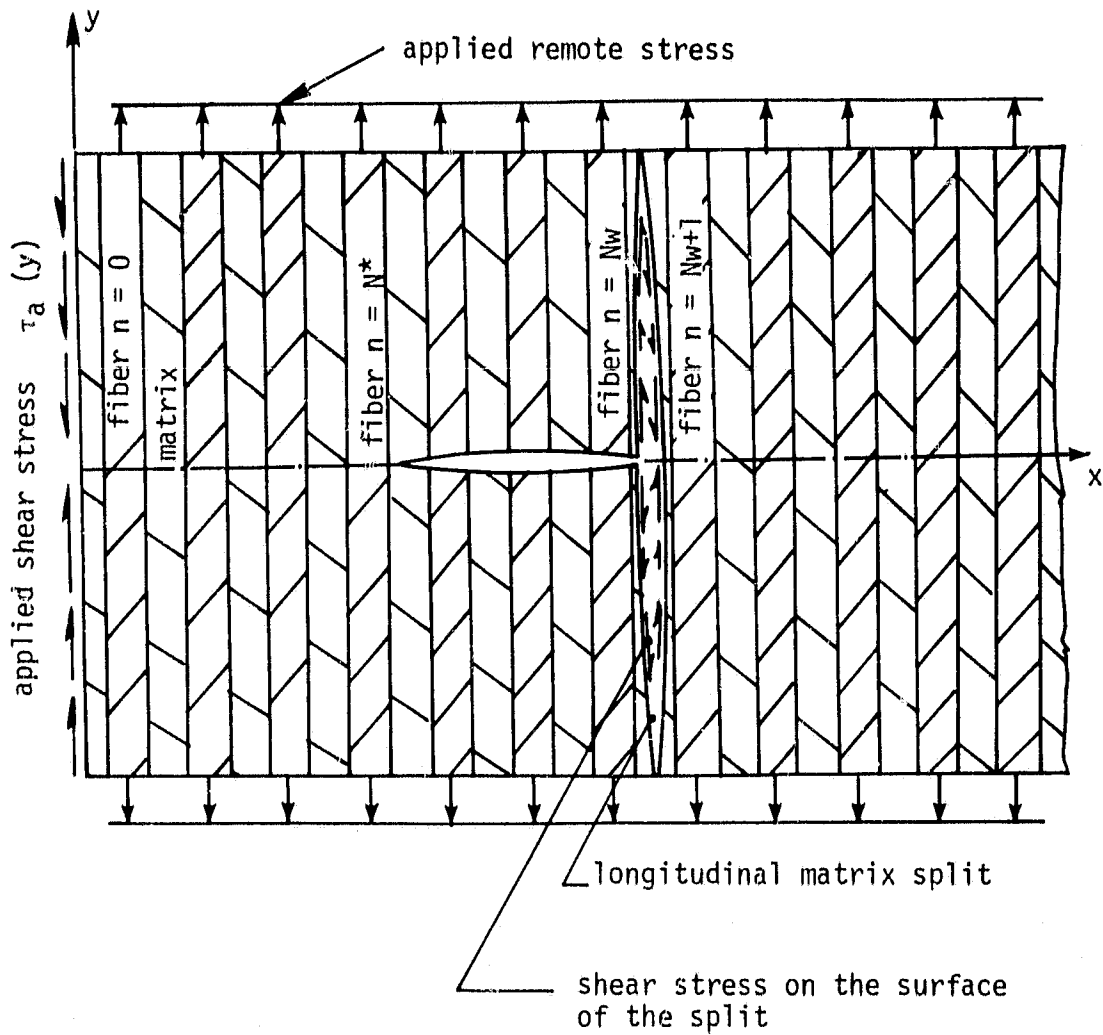
Figure 6. Half-Plane with Matrix Split

$$\sum_{m=1}^{M_2} B_m^{II} \frac{2}{\pi} \int_0^\pi \cos[(N_2^* + m + \frac{1}{2})\theta]\cos[(n+\frac{1}{2})\theta]d\theta$$

$$+ \frac{2}{\pi} \int_0^\pi \cos(\theta/2)\cos[(n+\frac{1}{2})\theta] \int_0^\infty e^{-\delta t} \bar{\tau}_a^{II}(t)dt \, d\theta$$

$$+ \frac{2}{\pi} \int_0^\pi F^2 \cos[(n+\frac{1}{2})\theta] \int_0^\infty e^{-\delta s}\left\{g(s) - \bar{\tau}_b^{II}(s)\right\} ds \, d\theta = 1, \quad (42)$$

for all broken fibers.

If $\bar{\tau}_a^{II}(s)$, $g(t)$ and $\bar{\tau}_b^{II}(s)$ are known, Equation (42) reduces to a set of linear algebraic equations in B_m^{II} and can be solved directly.

When the above finite strip, region II, is introduced between the two half-planes, planes I and III, as shown in Figure 5, it results in two interfaces each similar to the one discussed in the problem of adjoined half-planes. The interfacial shear stresses $\bar{\tau}_a^{I}(\eta)$, $\bar{\tau}_a^{II}(\xi)$, $\bar{\tau}_b^{II}(\xi)$ and $\bar{\tau}_b^{III}(\zeta)$ can be obtained in the same manner as in the previous solution, that is, using the following relations:

$$\tau_a^{I}(y) = - \tau_a^{II}(y), \quad \text{and}$$

$$\tau_a^{I}(y) = (G_M/h)^{i1} [v_0^{I}(y) - v_0^{II}(y)], \quad \text{between planes I and II}, \quad (43)$$

and

$$\tau_b^{II}(y) = \tau_b^{III}(y), \quad \text{and}$$

$$\tau_b^{II}(y) = -(G_M/h)^{i2} [v_{Nw}^{II}(y) - v_0^{III}(y)] \quad \text{between planes II and III}, (44)$$

where $(G_M/h)^{i1}$ and $(G_M/h)^{i2}$ are the shear stiffnesses of the respective interfaces. By definition $g(\xi)$ is given by

$$g(\xi) = V_{Nw+1}^{II} - V_{Nw}^{II} . \quad (45)$$

Equations (43) - (45) along with the two equations for the Fourier constants from the stress boundary conditions on the broken fibers in region I and II, Equations (34) and (42), represent the complete solution for the

finite width buffer strip problem. In Equation (45) it must be noted that V_{Nw}^{II} is the normalized displacement of fiber Nw of the finite strip, whereas V_{Nw+1} is the normalized displacement of the first fiber of a new half-plane having applied shear stresses $\bar{\tau}_b^{II}(\xi)$ along the free edge and fiber/matrix properties of the finite strip.

As in the previous problem, first the actual displacements are substituted in terms of their corresponding normalized displacements, then the normalized displacements are substituted in terms of the normalized shear stresses and the Fourier constants. Further, $\bar{\tau}_a^{II}(\xi)$ and $\bar{\tau}_b^{III}(\zeta)$ can be eliminated knowing the relationship between the actual shear stresses, Equations (43) and (44). Then the final set of governing equations for the finite width buffer strip problem can be listed as follows:

$$\sum_{m=1}^{M_1} B_m^I \frac{2}{\pi} \int_0^\pi \cos[(N_1^* + m + \tfrac{1}{2})\theta]\cos[(n + \tfrac{1}{2})\theta]\delta d\theta$$

$$+ \frac{2}{\pi} \int_0^\pi \cos(\theta/2)\cos[(n + \tfrac{1}{2})\theta] \int_0^\infty e^{-\delta t} \bar{\tau}_a^I(t)dt\, d\theta = 1 , \qquad (46)$$

$$\sum_{m=1}^{M_2} B_m^{II} \frac{2}{\pi} \int_0^\pi \cos[(N_2^* + m + \tfrac{1}{2})\theta]\cos[(\ell + \tfrac{1}{2})\theta]\delta d\theta$$

$$- \frac{G_{12}}{R_1^2} \frac{2}{\pi} \int_0^\pi \cos(\theta/2)\cos[(\ell + \tfrac{1}{2})\theta] \int_0^\infty e^{-\delta_1 t} \bar{\tau}_a^I(t)dt\, d\theta$$

$$+ \frac{2}{\pi} \int_0^\pi F^2 \cos[(\ell + \tfrac{1}{2})\theta] \int_0^\infty e^{-\delta s} \left\{ g(s) - \bar{\tau}_b^{II}(s) \right\} ds\, d\theta = 1 , \qquad (47)$$

for $n = N_1^* + 1, \ldots, N_1$ and $\ell = N_2^* + 1, \ldots, N_2$,

$$\bar{\tau}_a^I(\eta) = \sum_{m=1}^{M_1} B_m^I G_{11} \frac{2}{\pi} \int_0^\pi \cos[(N_1^* + m + \tfrac{1}{2})\theta]\cos(\theta/2)e^{-\delta\eta}\, d\theta$$

$$- \sum_{m=1}^{M_2} B_m^{II} G_{11} R_1 \frac{2}{\pi} \int_0^\pi \cos[(N_2^* + m + \tfrac{1}{2})\theta]\cos(\theta/2)e^{-\delta_1\eta}\, d\theta$$

$$- \int_0^\infty \frac{G_{i1}}{\pi} \int_0^\pi \frac{\cos^2(\theta/2)}{\delta} [D(\delta,n,t) + G_{12} D(\delta_1,n,t)] d\theta \; \bar{\tau}_a^I(t) dt$$

$$+ \int_0^\infty G_{i1} \frac{R_1}{\pi} \int_0^\pi \frac{\cos(\theta/2)}{\delta} F^2 D(\delta,n/R_1,s) d\theta \; [g(s) - \bar{\tau}_b^{II}(s)] ds, \tag{48}$$

$$g(\xi) = - \sum_{m=1}^{M_2} B_m^{II} \frac{2}{\pi} \int_0^\pi \cos[(N_2^* + m + \tfrac{1}{2})\theta]\cos[(Nw + \tfrac{1}{2})\theta]e^{-\delta\xi} d\theta$$

$$- \int_0^\infty \frac{G_{12}}{R_1^2} \frac{1}{\pi} \int_0^\pi \frac{\cos(\theta/2)}{\delta} \cos[(Nw + \tfrac{1}{2})\theta] D(\delta,t/R_1,\xi) d\theta \; \bar{\tau}_a^I(t) dt$$

$$+ \int_0^\infty \frac{1}{\pi} \int_0^\pi \frac{\cos[(Nw + \tfrac{1}{2})\theta]}{\delta} F^2 D(\delta,\xi,s) d\theta \; g(s) ds$$

$$- \int_0^\infty \frac{1}{\pi} \int_0^\pi \left\{ \frac{\cos^2(\theta/2)}{\delta} + \frac{F^2\cos[(Nw + \tfrac{1}{2})\theta]}{\delta} \right\} D(\delta,\xi,s) d\theta \; \bar{\tau}_b^{II}(s) ds, \tag{49}$$

and

$$\bar{\tau}_b^{II}(\xi) = - \sum_{m=1}^{M_2} B_m^{II} G_{i2} \frac{2}{\pi} \int_0^\pi \cos[(N_2^* + m + \tfrac{1}{2})\theta]\cos[(Nw + \tfrac{1}{2})\theta]e^{-\delta\xi} d\theta$$

$$- \int_0^\infty \frac{G_{i2} G_{12}}{R_1^2} \frac{1}{\pi} \int_0^\pi \frac{\cos(\theta/2)}{\delta} \cos[(Nw + \tfrac{1}{2})\theta] D(\delta,t/R_1,\xi) d\theta \; \bar{\tau}_a^I(t) dt$$

$$+ \int_0^\infty \frac{G_{i2}}{\pi} \int_0^\pi \frac{\cos[(Nw + \tfrac{1}{2})\theta]}{\delta} F^2 D(\delta,\xi,s) d\theta \; g(s) ds$$

$$- \int_0^\infty \frac{G_{i1}}{\pi} \int_0^\pi \left[\frac{G_{23}}{R_2} \frac{\cos^2(\theta/2)}{\delta} D(\delta_2,\xi,s) \right.$$
$$\left. + \frac{\cos[(Nw + \tfrac{1}{2})\theta]}{\delta} F^2 D(\delta,\xi,s) \right] d\theta \; \bar{\tau}_b^{II}(s) ds \tag{50}$$

where

$$R_1 = \sqrt{\left(\frac{A_F E_F h}{G_M t}\right)^{II} \left(\frac{G_M t}{A_F E_F h}\right)^{I}} \quad,$$

$$R_2 = \sqrt{\left(\frac{A_F E_F h}{G_M t}\right)^{III} \left(\frac{G_M t}{A_F E_F h}\right)^{II}} \quad,$$

$$\delta_1 = \delta/R_1 \quad ,$$

$$\delta_2 = \delta/R_2 \quad ,$$

$$G_{i1} = (G_M/h)^{i1}(h/G_M)^{I} \quad ,$$

$$G_{i2} = (G_M/h)^{i2}(h/G_M)^{II} \quad , \quad \text{and}$$

$$G_{23} = (G_M/h)^{II}(h/G_M)^{III} \quad .$$

The solution reduces to two series equations and three linear integral equations.

Uni-Directional Finite Width Strip with Broken Fibers

In this section a solution is obtained for a uni-directional finite width strip containing an arbitrary number of broken fibers as a special case of the solutions already developed. With reference to Figure 5 it can be seen that if the interfacial shear stresses $\tau_a^{II}(y)$ and $\tau_b^{II}(y)$ acting on the region II are zero then it results in a finite width strip with broken fibers subjected to a uniform remote axial stress as shown in Figure 7. Therefore the solution to the finite width strip problem can be obtained as a special case of the solution developed for region II of the buffer strip laminate by setting $\bar{\tau}_a^{II}(t)$ and $\bar{\tau}_b^{II}(s)$ to zero in Equations (42). With reference to Figure 7 these equations are given as

$$\sum_{m=1}^{M} B_m \frac{2}{\pi} \int_0^\pi \cos[(N^* + m + \tfrac{1}{2})\theta]\cos[(n + \tfrac{1}{2})\theta]d\theta$$

$$+ \frac{2}{\pi} \int_0^\pi F^2 \cos[(n + \tfrac{1}{2})\theta] \int_0^\infty e^{-\delta t} g(t)dt \, d\theta = 1 \quad , \qquad (51)$$

for all broken fibers, and

$$g(\xi) = - \sum_{m=1}^{M} B_m \frac{2}{\pi} \int_0^\pi \cos[(N^* + m + \tfrac{1}{2})\theta]\cos[(Nw + \tfrac{1}{2})\theta] \, e^{-\delta\xi} \, d\theta$$

$$+ \int_0^\infty \frac{2}{\pi} \int_0^\pi \frac{\cos[(Nw + \tfrac{1}{2})\theta]}{\delta} F^2 \, D(\delta,\xi,t)d\theta \, g(t)dt \qquad (52)$$
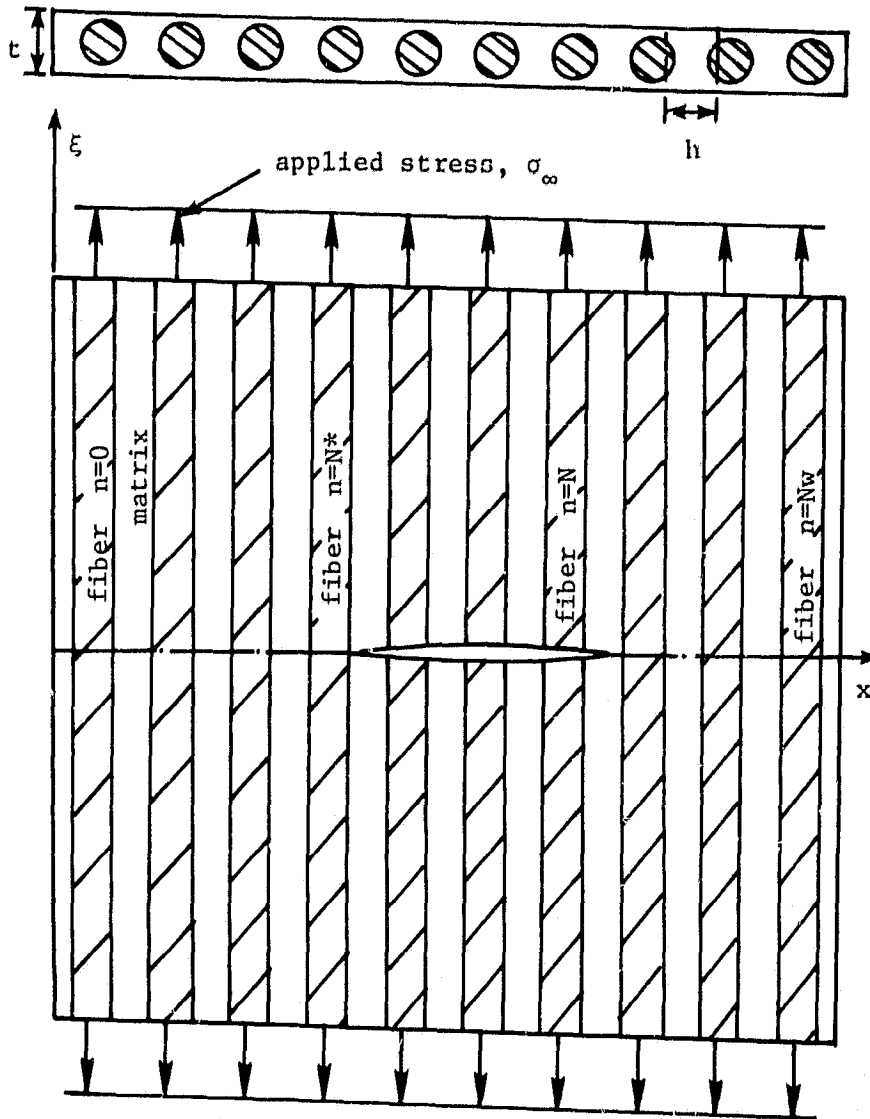
Figure 7. Finite Width Uni-Directional Strip

where

$$F^2 = \cos[(N_w + \tfrac{1}{2})\theta] - \cos[(N_w + \tfrac{3}{2})\theta] \ , \quad \text{and}$$

$$g(\xi) = V_{N_w+1} - V_{N_w} \ .$$

Since by definition V_{N_w+1} is the displacement of the first fiber of a new half-plane having fiber/matrix properties of the finite width strip and no applied shear stress along the free edge, it must be equal to zero. Therefore $g(\xi)$ is given by

$$g(\xi) = - V_{N_w} \ . \tag{53}$$

Therefore the solution of the finite width strip reduces to one series equation coupled with one linear integral equation. The location and the number of broken fibers are arbitrary except that the fiber breaks must be along the x-axis. The solution obtained holds for a central notch, an edge notch, an off-center notch, or for multiple notches along the x-axis.

CHAPTER III

SOLUTION TECHNIQUE

In all the problems dealt with so far, the solution reduces to one or two series equations coupled with one or more linear Fredholm integral equations of the second kind. Since there is no exact closed form solution available to solve such a system of equations, a numerical procedure is developed and presented in this section. The technique makes use of a method given by Riez [12], to solve a linear Fredholm integral equation of the second kind defined within a semi-infinite interval of integration. The solution is based on the fact that a given integral over a semi-infinite interval may be approximated by the Gauss-Laguerre quadrature rule as

$$\int_0^\infty f(x)dx = \sum_{i=1}^{k} w_i\, e^{-x_i} f(x_i) \tag{54}$$

where x_i is the ith zero of the Laguerre polynomial, $L_k(x)$, and w_i is the corresponding weight function given by

$$w_i = \frac{x_i}{[(k+1)\, L_{k+1}(x_i)]^2} \ . \tag{55}$$

The Laguerre polynomial $L_k(x)$ is given by

$$L_k(x) = e^x \frac{d^k(x^k e^{-x})}{dx^k} \ . \tag{56}$$

Since the form of the equations for each of the solutions is the same, the development and application of the numerical procedure can be demonstrated, without loss of generality, by taking the equations corresponding to one of the solutions. Consider then the solution corresponding to the problem of adjoined half-planes given by Equations

$$\sum_{m=1}^{M_1} B_m^I \frac{2}{\pi} \int_0^\infty \cos[(N_1^* + m + \tfrac{1}{2})\theta]\cos[(n + \tfrac{1}{2})\theta]\delta d\theta$$

$$+ \frac{2}{\pi} \int_0^\pi \cos(\theta/2)\cos[(n + \tfrac{1}{2})\theta] \int_0^\infty e^{-\delta t} \bar{\tau}_a^I(t)dt \, d\theta = 1 \,, \qquad (57)$$

$$\sum_{m=1}^{M_2} B_m^{II} \frac{2}{\pi} \int_0^\pi \cos[(N_2^* + m + \tfrac{1}{2})\theta]\cos[(\ell + \tfrac{1}{2})\theta]\delta d\theta$$

$$- \frac{G_{12}}{R_1^2} \frac{2}{\pi} \int_0^\pi \cos(\theta/2)\cos[(\ell + \tfrac{1}{2})\theta] \int_0^\infty e^{-\delta_1 t} \tau_a^I(t)dt \, d\theta = 1 \,, \qquad (58)$$

for $n = N_1^* + 1,\ldots,N_1$ and $\ell = N_2^* + 1,\ldots,N_2$, and

$$\bar{\tau}_a^I(\eta) = G_{11} \frac{2}{\pi} \int_0^\pi \sum_{m=1}^{M_1} B_m^I \cos[(N_1^* + m + \tfrac{1}{2})\theta]\cos(\theta/2)e^{-\delta\eta} \, d\theta$$

$$- R_1 G_{11} \frac{2}{\pi} \int_0^\pi \sum_{m=1}^{M_2} B_m^{II} \cos[(N_2^* + m + \tfrac{1}{2})\theta]\cos(\theta/2)e^{-\delta_1\eta} \, d\theta$$

$$- G_{11} \int_0^\pi \frac{2}{\pi} \int_0^\pi \frac{\cos^2(\theta/2)}{\delta} \left[D(\delta,\eta,t) + \frac{G_{12}}{R_1} D(\delta_1,\eta,t) \right]$$

$$\times d\theta \, \bar{\tau}_a^I(t)dt \,. \quad (59)$$

Integrals over the spatial variable, t, in the above equations, defined over the semi-infinite interval, can now be replaced by the above series representation to yield

$$\sum_{m=1}^{M_1} \left\{ \frac{2}{\pi} \int_0^\pi \cos[(N_1^* + m + \tfrac{1}{2})\theta]\cos[(n + \tfrac{1}{2})\theta]\delta d\theta \right\} B_m^I$$

$$+ \sum_{j=1}^{k} \left\{ \frac{2}{\pi} \int_0^\pi \cos(\theta/2)\cos[(n + \tfrac{1}{2})\theta]e^{-\delta t_j} \, d\theta \, w_j e^{t_j} \right\} \bar{\tau}_a^I(t_j) = 1 \qquad (60)$$

$$\sum_{m=1}^{M_2} \left\{ \frac{2}{\pi} \int_0^\pi \cos[(N_2^* + m + \tfrac{1}{2})\theta]\cos[(\ell + \tfrac{1}{2})\theta]\delta d\theta \right\} B_m^{II}$$

$$-\sum_{j=1}^{k}\left\{\frac{G_{12}}{R_1^2}\frac{2}{\pi}\int_0^{\pi}\cos(\theta/2)\cos[(\ell+\tfrac{1}{2})\theta]e^{-\delta_1 t_j}\,d\theta\; w_j e^{t_j}\right\}\bar{\tau}_a^{I}(t_j)=1,$$

(61)

for $n = N_1^* + 1,\ldots,N_1$, and $\ell = N_2^* + 1,\ldots,N_2$, and

$$\left\{\delta_{ij} + \sum_{j=1}^{k} K(n_i,t_j)w_j e^{t_j}\right\}\bar{\tau}_a^{I}(t_j)$$

$$-\sum_{m=1}^{M_1}\left\{G_{11}\frac{2}{\pi}\int_0^{\pi}\cos[(N_1^*+m+\tfrac{1}{2})\theta]\cos(\theta/2)e^{-\delta n_i}\,d\theta\right\}B_m^{I}$$

$$+\sum_{m=1}^{M_2}\left\{R_1 G_{11}\frac{2}{\pi}\int_0^{\pi}\cos[(N_2^*+m+\tfrac{1}{2})\theta]\cos(\theta/2)e^{-\delta_1 n_i}\,d\theta\right\}$$

$$\times B_m^{II} = 0, \qquad i = 1,\ldots,k \qquad (62)$$

where, $\delta_{ij} = 1$ for $i = j$

$\qquad\qquad = 0$ for $i \neq j$,

and $K(n_i,t_j) = \dfrac{2G_{11}}{\pi}\int_0^{\pi}\dfrac{\cos^2(\theta/2)}{\delta}[D(\delta,n_i,t_j) + \dfrac{G_{12}}{R_1}D(\delta_1,n_i,t_j)]d\theta$.

Therefore, the solution of the integral equation coupled with a set of series equations reduces to solving a system of linear algebraic equations in B_m^{I}, B_m^{II} and explicit values of $\bar{\tau}_a^{I}(n)$ at the quadrature points. The above system of equations is solved by the method of Gauss-elimination with partial pivoting.

It must be pointed out that the terms in the integral equation of the form $e^{-\delta|n-t|}$ have cusp at $n = t$ and the quadrature representation in the standard form, Equation (54), results in large inaccuracies especially for large values of n. This has been overcome by modifying the above quadrature rule by deleting selected terms in the series and replacing them by closed form integration in the neighborhood of the cusp. With reference to Figure 8, the integral over the semi-infinite interval is then represented by the modified equation
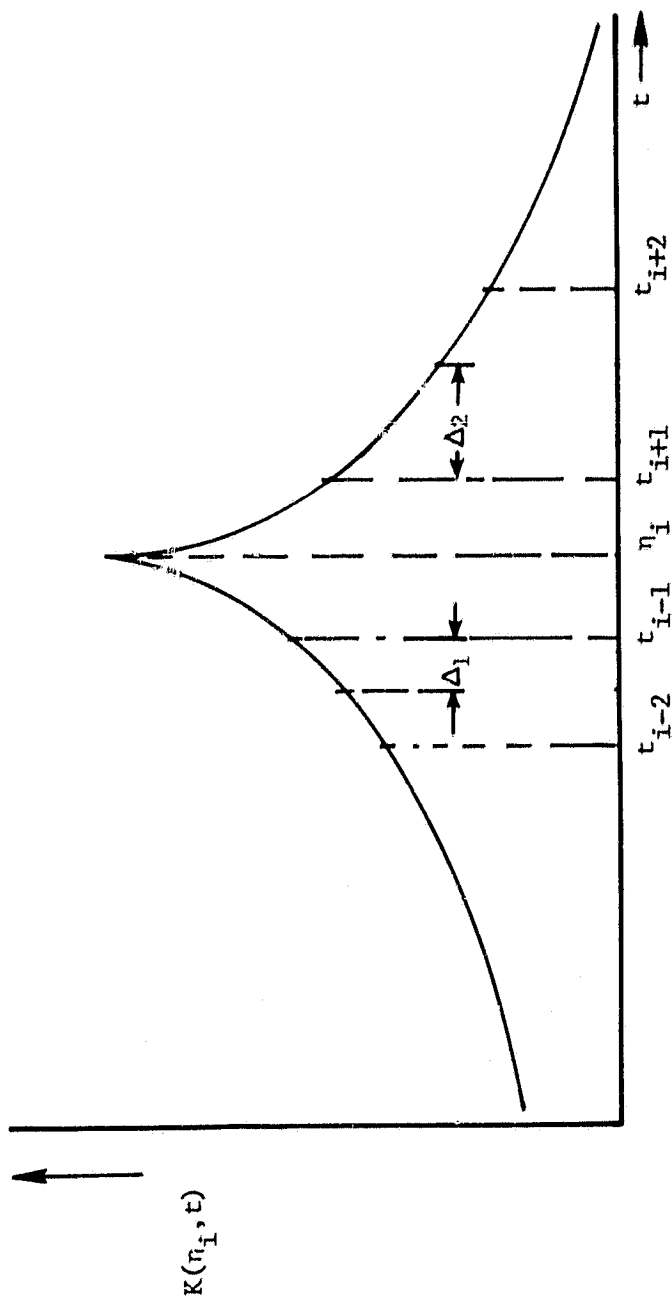
Figure 8.   Integrand with a Cusp

$$\int_0^\infty K(n_i,t)\,\bar{\tau}_a^I(t)dt = \sum_{j=1}^k K(n_i,t_j)\,\bar{\tau}_A^I(t_j)e^{t_j} w_j$$

$$- \left[K(n_i,t_{i-1})\,\bar{\tau}_a^I(t_{i-1})e^{t_{i-1}} w_{i-1} + K(n_i,t_i)\,\bar{\tau}_a^I(t_i)e^{t_i} w_i \right.$$

$$\left. + K(n_i,t_{i+1})\,\bar{\tau}_a^I(t_{i+1})e^{t_{i+1}} w_{i+1} \right]$$

$$+ \left[\int_{t_{i-1}-\Delta_1}^{t_i} K(n_i,t)\,\bar{\tau}_a^I(t)dt + \int_{t_i}^{t_{i+1}+\Delta_2} K(n_i,t)\,\bar{\tau}_a^I(t)dt \right] \qquad (63)$$

where,

$$\Delta_1 = (t_{i-1} - t_{i-2})/2 \quad , \quad \text{and}$$

$$\Delta_2 = (t_{i+2} - t_{i+1})/2 \quad .$$

Since $\bar{\tau}_a^I(t)$ is yet unknown, the two integrals on the right hand side of Equation (63) can not be evaluated in a closed form. However, if the function $\bar{\tau}_a^I(t)$ is taken to be the average of the terminal values within each of the intervals, the above two integrals can be expressed as

$$\int_{t_{i-1}-\Delta_1}^{t_i} K(n_i,t)\,\bar{\tau}_a^I(t)dt = \frac{[\bar{\tau}_a^I(t_{i-1}) + \bar{\tau}_a^I(t_i)]}{2} \int_{t_{i-1}-\Delta_1}^{t_i} K(n_i,t)dt \quad ,$$

and

$$\int_{t_i}^{t_{i+1}+\Delta_2} K(n_i,t)\,\bar{\tau}_a^I(t)dt = \frac{[\bar{\tau}_a^I(t_i) + \bar{\tau}_a^I(t_{i+1})]}{2} \int_{t_i}^{t_{i+1}+\Delta_2} K(n_i,t)dt \quad . \ (64)$$

Substituting Equation (64) into Equation (63) and rewriting results in

$$\int_0^\infty K(n_i,t)\,\bar{\tau}_a^I(t)dt = \sum_{j=1}^{k}{}^* K(n_i,t)\,\bar{\tau}_a^I(t_j)e^{t_j} w_j$$

$$+ \frac{1}{2}\int_{t_{i-1}-\Delta_1}^{t_i} K(n_i,t)dt\ \bar{\tau}_a^I(t_{i-1})$$

$$+ \frac{1}{2} \left[\int_{t_{i-1}-\Delta_1}^{t_i} K(n_i,t)dt + \int_{t_i}^{t_{i+1}+\Delta_2} K(n_i,t)dt \right] \bar{\tau}_a^I(t_i)$$

$$+ \frac{1}{2} \int_{t_i}^{t_{i+1}+\Delta_2} K(n_i,t)dt \ \bar{\tau}_a^I(t_i) \ , \tag{65}$$

where Σ^* excludes terms corresponding to $j = i-1$, i and $i+1$.

The quadrature-rule in the modified form, Equation (65), is used to represent those integrals in which the integrand has terms with cusp. The two series equations remain unaltered and the substitution of Equation (65) into Equation (59) results in

$$\sum_{j=1}^{k}{}^* K(n_i,t_j)w_j \ e^{t_j} \ \bar{\tau}_a^I(t_j) + a_{i-1} \ \bar{\tau}_a^I(t_{i-1}) + (1+a_i)\bar{\tau}_a^I(t_i) + a_{i+1} \ \bar{\tau}_a^I(t_{i+1})$$

$$- \sum_{m=1}^{M_1} \left\{ G_{i1} \frac{2}{\pi} \int_0^\pi \cos[(N_1^* + m + \frac{1}{2})\theta]\cos(\theta/2)e^{-\delta n_i}d\theta \right\} B_m^I$$

$$+ \sum_{m=1}^{M_2} \left\{ R_1 G_{i1} \frac{2}{\pi} \int_0^\pi \cos[(N_2^* + m + \frac{1}{2})\theta]\cos(\theta/2)e^{-\delta_1 n_i} d\theta \right\}$$

$$\times \ B_m^{II} = 0 \ , \qquad i = 1,\dots,k \ . \tag{66}$$

where,

$$a_{i-1} = \frac{1}{2} \int_{t_{i-1}-\Delta_1}^{t_i} K(n_i,t)dt \ ,$$

$$a_i = \frac{1}{2} \int_{t_{i-1}-\Delta_1}^{t_i} K(n_i,t)dt + \frac{1}{2} \int_{t_i}^{t_{i+1}+\Delta_2} K(n_i,t)dt \ , \quad \text{and}$$

$$a_{i+1} = \frac{1}{2} \int_{t_i}^{t_{i+1}+\Delta_2} K(n_i,t)dt \ .$$

This again reduces to solving set of linear algebraic equations as before.

CHAPTER IV

RESULTS AND CONCLUSIONS

First, typical results are given for a Graphite/epoxy laminate containing a buffer strip as shown in Figure 9. The crack growth behavior of the lamina is studied by varying the buffer strip material, the width and the thickness of the strip and the initial crack length. The three materials considered for the buffer strip are Nylon, Kevlar and S-glass, all in an epoxy matrix. The matrix and fibers are assumed to be linearly elastic. The failure criterion is that a fiber fails upon reaching its ultimate failure stress as determined from an unnotched coupon test.

Figure 10 presents results corresponding to initial crack growth in plane I, crack arrest at the interface, crack growth in the buffer strip and subsequent lamina failure. In these results all fibers are of the same cross-sectional area and in all cases the buffer strip is ten fibers wide. Since all the buffer strip candidate materials are of lower modulus than that of the parent laminate, which in this case is Graphite/epoxy, the stress concentration factor at the near end of the notch (nearer to the interface) is always higher than that at the far end of the notch. The solid line in Figure 10 represents the remote stress required to initiate crack extension, (fail the first unbroken fiber in front of the notch, fiber A in Figure 9). The remote stress required to fail the lamina catastrophically, (fail the first fiber in plane III, fiber B in Figure 9) is given by the broken line in Figure 10. Both these stresses are functions of the initial crack length and decrease with increasing length. The crack growth takes place by breaking
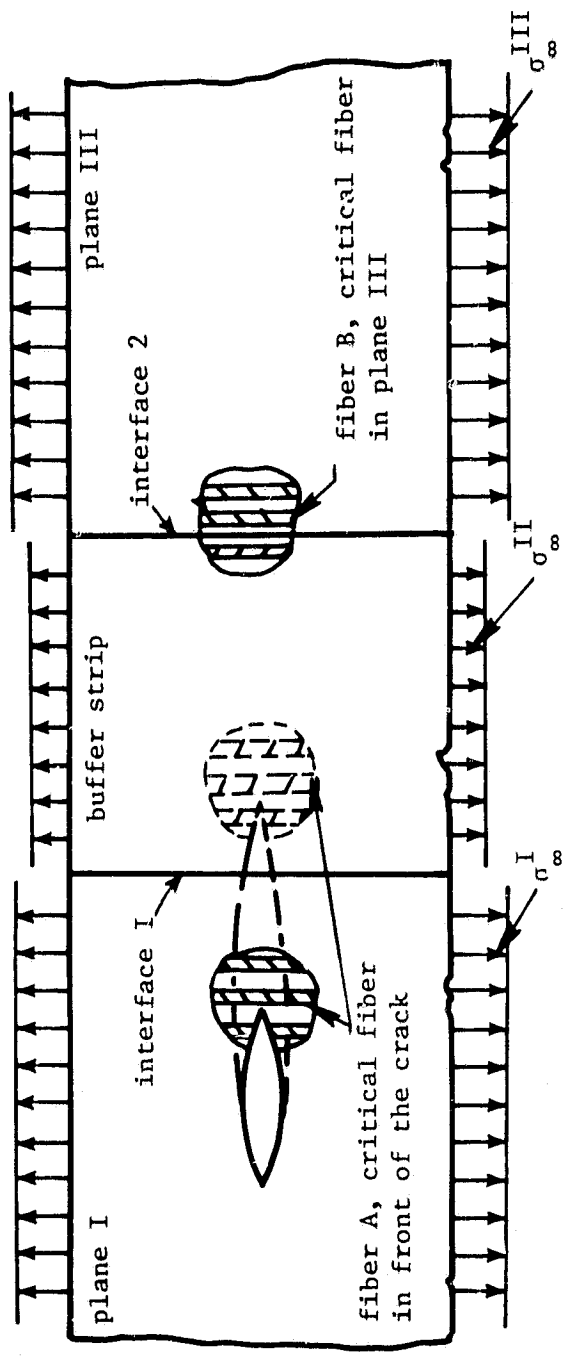
Figure 9. Buffer Strip Laminate with Initial Damage

consecutive fibers from the crack tip to the interface. Then, depending on the stress level required to run the crack to the interface and depending on the buffer strip material, the crack may arrest. It is very interesting to note that all three buffer strip materials require an increasing stress to continue the crack growth in the buffer strip, although Kevlar will only arrest a crack if it initiates under fairly low load, i.e. initially close to the interface.

Total lamina failure will occur when either the buffer strip is fully broken or when the first fiber in plane III, fiber B, fails. In both cases continued crack growth is unstable once fiber B fails. For the particular lamina of Figure 9, all fibers in the Kevlar buffer strip fail before fiber B attains its failure stress, whereas for S-glass and Nylon, fiber B fails when there are still some fibers left unbroken, i.e., the crack jumps the buffer strip. The ultimate lamina failure stresses are

$\sigma_\infty = 0.272 \, \sigma_{ult}$ for Kevlar

$\sigma_\infty = 0.395 \, \sigma_{ult}$ for S-glass, and

$\sigma_\infty = 0.444 \, \sigma_{ult}$ for Nylon,

where σ_{ult} is the ultimate fiber stress as determined from an unnotched Graphite/epoxy laminate. The material properties used for these results are given in Table 1. The results of Figure 10 indicate Nylon to be the best of the three materials but this is only true if the matrix can support the very large failure strains (about 20%) of Nylon. In a typical angle-ply laminate with Nylon buffer strips and with continuous ±45 graphite plies, high strain levels certainly cannot be reached before failing the angle-plies and continuing the crack. This behavior was observed by Verrette and Labor [4]. The extension of this study to
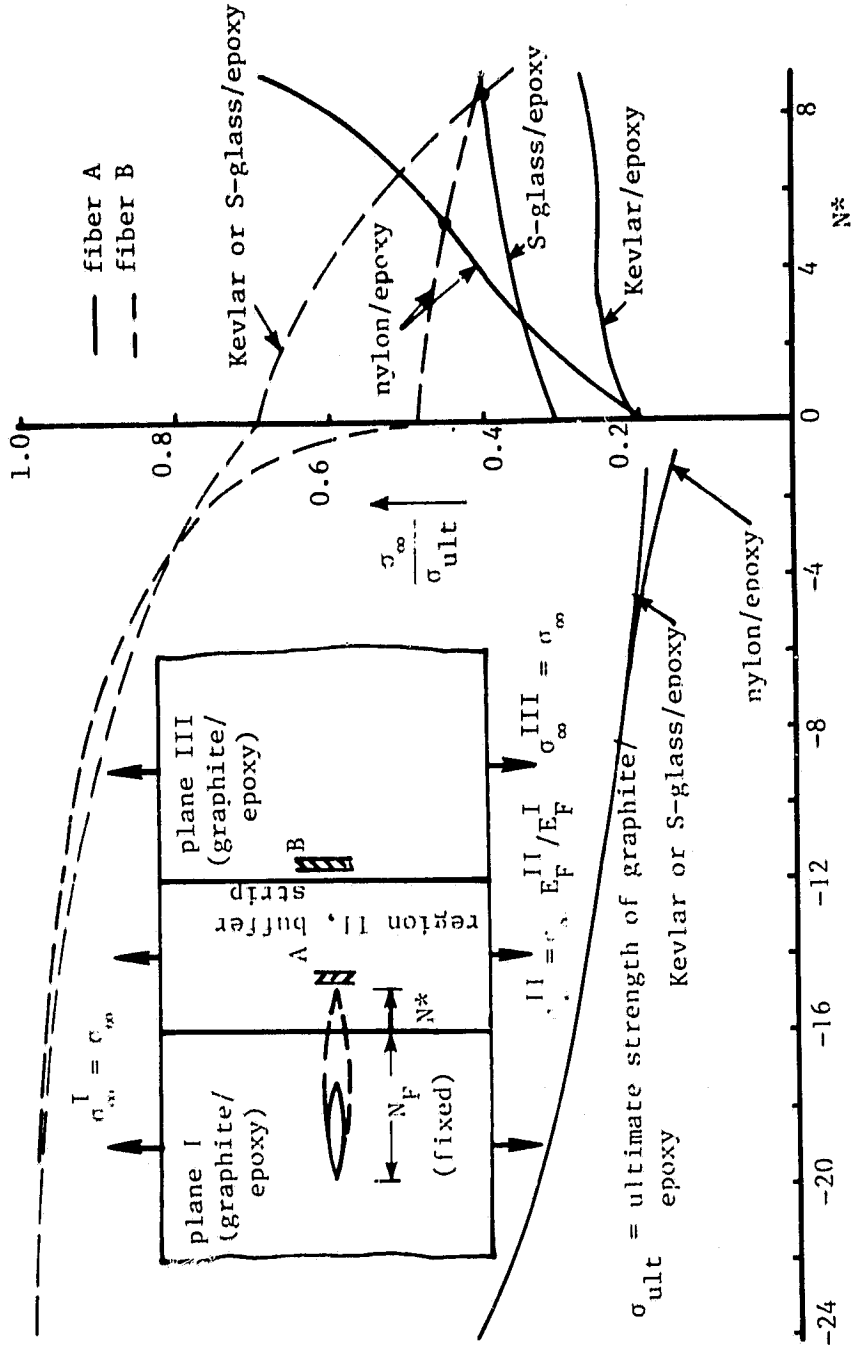
Figure 10. Failure Stress as a Function of Crack Growth

account for angle plies is surely necessary to represent accurately such low modulus fibers.

TABLE 1. FIBER PROPERTIES

fiber	mass density Gms/m^3	modulus MPa	ult. stress MPa
Nylon	84	2000	233
Kevlar	106	111400	2020
S-glass	199	101000	2800
Graphite	155	300000	2800

In Figures 11-13 the effect of buffer strip width on crack growth through the strip is indicated. The ultimate failure stress of the lamina as a function of buffer strip width is plotted in Figure 14. From Figure 14 it is seen that for Nylon the ultimate failure stress continues to increase with an increase in width, whereas for S-glass and Kevlar about ten fiber widths is optimum.

Table 2 gives a comparison of the ultimate lamina failure stress for a buffer strip of ten fibers, first for equal area and then for equal weights of the fibers. These results are normalized with respect to S-glass. A Kevlar region of two plies is approximately equivalent to one ply of S-glass in weight and it is seen that S-glass is still superior to Kevlar. This agrees with results obtained by Poe and Kennedy [5].

Next, results are presented for the finite width strip with broken fibers forming a central notch and subjected to a uniform remote axial stress as shown in Figure 7. The stress concentration factors for various notch lengths (number of broken fibers, M) are obtained corresponding to
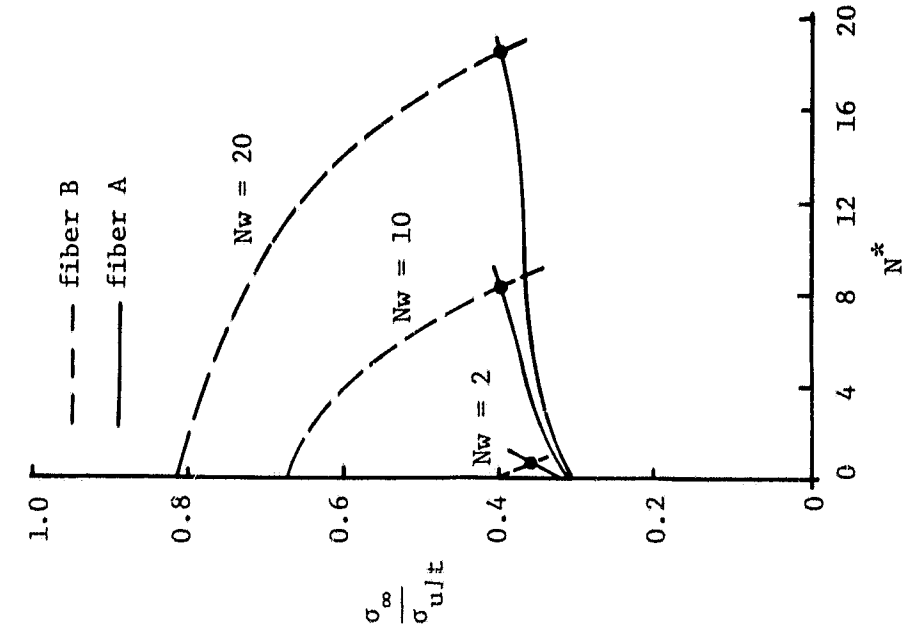
Figure 12. Effect of Buffer Strip Width on Crack Growth (S-Glass)
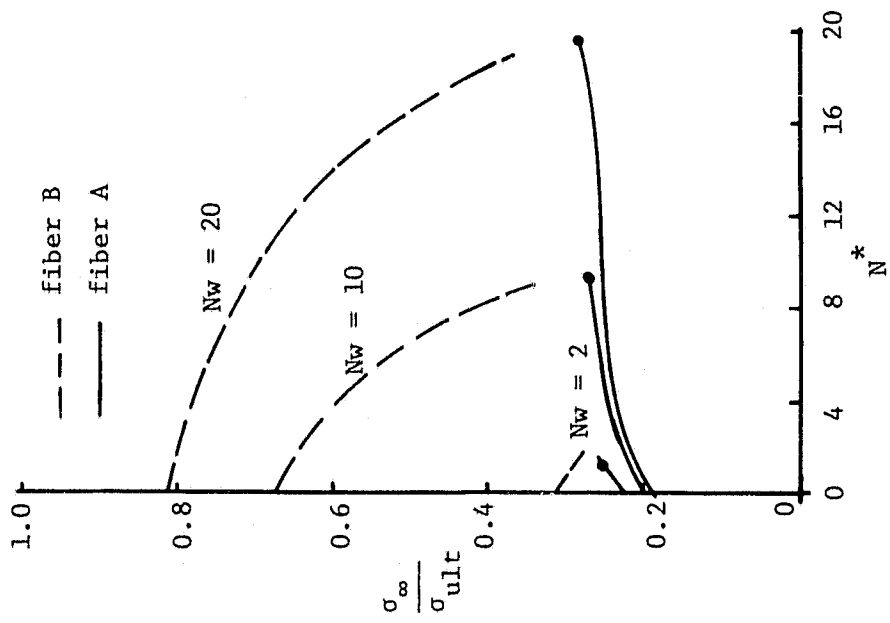

Figure 11. Effect of Buffer Strip Width on Crack Growth (Kevlar)
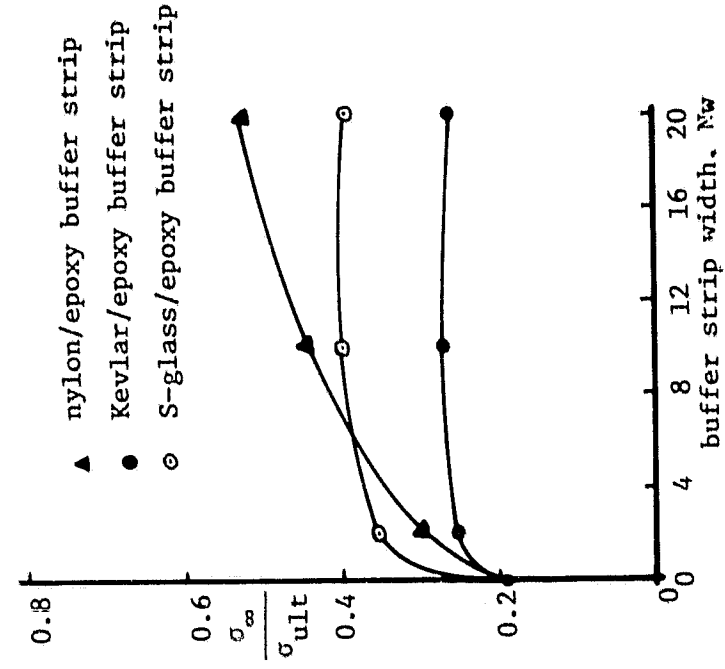
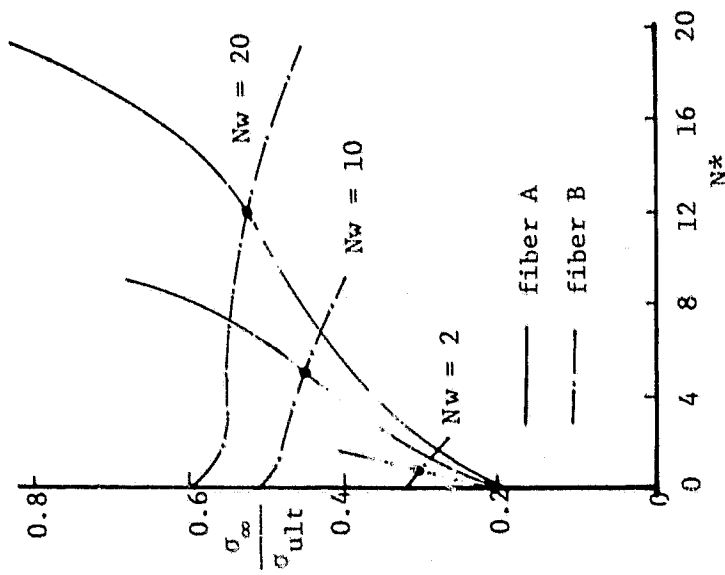Figure 14.   Ultimate Lamina Failure Stress
Vs. Buffer Strip Width

Figure 13.   Effect of Buffer Strip Width
on Crack Growth (Nylon)

TABLE 2.   COMPARISON OF LAMINA FAILURE STRESS

fiber	$\sigma_\infty/\sigma_{ult}$ equal area	$\sigma_\infty/\sigma_{ult}$ equal weight
Nylon	0.444	0.472
Kevlar	0.272	0.318
S-glass	0.395	0.395

two widths, Nw = 24 and 48.   Following Hedgepeth [6] the stress concentration factors for a uni-directional infinite region are obtained using the relation

$$\bar{\sigma}_{N+1} = \frac{\sigma_{N+1}}{\sigma_\infty} = \frac{4\cdot6\cdot8\cdot\ \cdot\ \cdot\ \cdot\ \cdot\ \cdot(2M+2)}{3\cdot5\cdot7\cdot\ \cdot\ \cdot\ \cdot\ \cdot\ \cdot(2M+1)} \qquad (67)$$

where

N+1   =   index of the first unbroken fiber at the notch tip,

M   =   total number of broken fibers in the notch,

$\bar{\sigma}_{N+1}$ =   stress concentration in fiber N+1,

σ_{N+1} =   axial stress in fiber N+1,   and

σ_∞ =   applied remote stress.

By comparing the above two stress concentration factors corresponding to a given notch length the finite width correction factor for a uni-directional strip is obtained and is given in Table 3.   Also given in Table 3 are the corresponding finite width correction factors for an isotropic strip obtained from the following relation [13]

$$Y_2 = 1.0 + 0.1282\ (2a/W) - 0.2881\ (2a/W)^2 + 1.5254\ (2a/W)^3, \qquad (68)$$
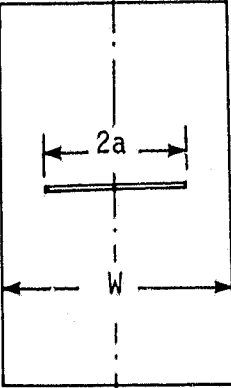
where,

Y_2 =   finite width correction factor,
a   =   half-crack length,   and
W   =   width of the strip.

From Table 3 it is seen that the finite width correction factors for the isotropic strip and the uni-directional strip are not significantly different for aspect ratios (notch length to strip width ratios) less than 0.5. For higher values of aspect ratios there is a considerable difference between the two cases. An aspect ratio of 0.9167 corresponds to 22 broken fibers in the 24 fiber strip and all the applied load is carried by the two remaining intact fibers giving a stress concentration factor of 11.0, (22 x 1.0/2). Similarly, the other limiting case corresponding to the aspect ratio of 0.9583 in which 46 fibers are broken out of 48, leaving the two end fibers to carry all the applied load giving a stress concentration of 23.0 (46/2). These two limiting cases are predicted accurately by the above solution indicating the validity of the model.

TABLE 3. FINITE WIDTH CORRECTION FACTORS

	2a/W	Finite width correction factors		
		uni-directional strip		Isotropic
		Nw = 24	Nw = 48	
2a = M x d W = Nw x d d=fiber spacing	0.1667	1.01334	1.01125	1.02042
	0.25	1.02890	1.02514	1.03788
	0.3333	1.05207	1.04581	1.06722
	0.5	1.13040	1.11598	1.18275
	0.75	1.44760	1.39280	1.57762
	0.9167	2.57412	3.7	2.05049
	0.9583	——	3.77560	2.20070

From the above results and discussions the following conclusions can be made. The method predicts the fracture behavior of a hybrid laminate in terms of material properties, geometry and initial crack length. The results agree well with those obtained experimentally for buffer strips of high modulus fibers such as S-glass and Kevlar, where the stiffness of the angle-plies is very small compared to that of zero degree ply. For low modulus (high failure strain) buffer strip materials such as Nylon, in which the stiffness of continuous angle-plies is comparable to that of the axial buffer strip fibers, the model is inadequate due to the basic assumption made in idealizing the laminate as a uni-directional composite. The method predicts the best buffer strip material to be one with a low modulus and as large an ultimate strength as possible, e.g., S-glass is superior to Kelvar.

As stated earlier, the main aim of this work was to understand the basic mechanism of crack growth and arrest in hybrid laminates, keeping the model as simple as possible. This goal has been achieved. However, in order to represent an actual buffer strip panel more realistically, the model certainly needs and has the potential for, further modifications. An immediate extension is to model the panel as a periodic uni-directional hybrid laminate simulating the regular placement of the buffer strips. Next, the role of angle plies must be accounted by either adding a cover sheet over the uni-directional laminate or by some other means. Finally, the effect of matrix damage in the form of longitudinal yielding and splitting at the crack tip and at the interfaces must be incorporated.

LIST OF REFERENCES

1. Eisemean, J. R. and Kaminski, B. E. "Fracture Control for Composite Structures." Engr. Fracture Mechs., Vol. 4, 1972, pp. 907-913.

2. Hess, T. E., Huang, S. L. and Rubin, H. "Fracture Control in Composite Materials Using Integral Crack Arresters." Proceedings of AIAA/ ASME/SAE 17th Structures, Structural Dynamics, and Materials Conference, May 5-7, 1976, pp. 52-60.

3. Avery, J. G. and Porter, T. R. "Damage Tolerant Structural Concepts for Fiber Composites." Proceedings of the Army Symposium on Solid Mechanics, 1976. "Composite Materials: The Influence of Mechanics of Fracture on Design." AMMRC-MS-76-2, 1976.

4. Verette, R. M. and Labor, J. D. "Structural Criteria for Advanced Composites." AFFDL-TR-76-142, Air Force Flight Dynamics Laboratory, 1976.

5. Poe, C. C., Jr., and Kennedy, J. M. "An Assessment of Buffer Strip for Improving Damage Tolerance of Composite Laminates." Jour. Comp. Mat. Supp., Vol. 14, pp. 57-70.

6. Hedgepeth, J. M. "Stress Concentrations in Filamentary Structures." NASA TN D-882, May 1961.

7. Hedgepeth, J. M. and Van Dyke, P. "Local Stress Concentrations in Imperfect Filamentary Composite Materials." Jour. Comp. Mat., Vol. 1, 1967, pp. 294-309.

8. Hedgepeth, J. M. and Van Dyke, P. "Stress Concentrations from Single-Filament Failures in Composite Materials." Textile Res., Vol. 29, 1969, pp. 618-626.

9. Goree, J. G. and Gross, R. S. "Analysis of a Uni-Directional Composite Containing Broken Fibers and Matrix Damage." Engr. Fracture Mechs. Vol. 13, 1979, pp. 563-578.

10. Goree, J. G., Dharani, L. R. and Jones, W. F. "Mathematical Modeling of Damage in Uni-Directional Composites." NASA CR 3453, 1981.

11. Dharani, L. R., Jones, W. F., and Goree, J. G. "Mathematical Modeling of Damage in Uni-Directional Composites." To be published, Engr. Fracture Mechs., Vol. 16, 1982.

12. Riez, A. "On the Numerical Solutions of Certain Types of Integral Equations." Arkiv for Mathematik, Astronomi Och Fysik, Vol. 29, No. 29, 1943, pp. 1-21.

13. Brown, W. F. and Strawley, J. E. "Plane Stain Crack Toughness of High Strength Metallic Materials." ASTM-STP 410, 1966.